Variable-Temperature Studies of Laser-Initiated $^5T_2 \rightarrow {}^1A_1$ Intersystem Crossing in Spin-Crossover Complexes: Empirical Correlations between Activation Parameters and Ligand Structure in a Series of Polypyridyl Ferrous Complexes

James K. McCusker,[1,2] Arnold L. Rheingold,[3] and David N. Hendrickson*[,1]

Department of Chemistry-0358, University of California, San Diego, California 92093-0358, and Department of Chemistry, University of Delaware, Newark, Delaware 19716

Received June 25, 1995[⊗]

Results are presented from a variable-temperature solution-phase laser photolysis study of the $^5T_2 \rightarrow {}^1A_1$ intersystem crossing in a series of related complexes: [Fe(tpen)]$(ClO_4)_2$, [Fe(tppn)]$(ClO_4)_2$, [Fe(tptn)]$(ClO_4)_2$, [Fe(*t*-tpchxn)]$(ClO_4)_2$, and [Fe$(dpa)_2$]$(ClO_4)_2$. The hexadentate ligands are formed with four 2-pyridylmethyl arms attached to ethylenediamine (tpen), 1,2-diaminopropylene (tppn), 1,3-diaminopropylene (tptn), or *trans*-1,2-diaminocyclohexane (*t*-tpchxn). The dpa ligand is a tridentate analogue of these ligands, namely, bis(2-pyridylmethyl)amine. The complex [Fe(mtpen)]$(ClO_4)_2 \cdot {}^2/_3H_2O$, where mtpen is the same as tpen except one of the pyridyl rings has a 6-methyl substituent, crystallizes in the space group $C2/c$, which at 173 K has a unit cell with $a = 41.390(13)$ Å, $b = 9.5239(16)$ Å, $c = 24.016(6)$ Å, $\beta = 108.24(3)°$, and $Z = 12$. Refinement with 2844 observed [$F > 5.0\sigma(F)$] reflections gave $R = 0.075$ and $R_w = 0.076$. The complex [Fe(tppn)]$(ClO_4)_2 \cdot {}^2/_3H_2O$ crystallizes in the space group $P2_1/n$, which at 296 K has a unit cell with $a = 12.979(4)$ Å, $b = 12.624(4)$ Å, $c = 19.475(6)$ Å, $\beta = 108.17(2)°$, and $Z = 4$. Refinement with 2357 observed [$F > 5.0\sigma(F)$] reflections gave $R = 0.1198$ and $R_w = 0.1141$. The mtpen complex is a high-spin Fe^{II} complex at all temperatures (4.2−400 K). The hydrated tpen complex is a spin-crossover complex with the temperature where there are 50% high-spin complexes ($T_{1/2}$) is ≃ 385 K, the hydrated tppn complex is also spin-crossover with a higher $T_{1/2}$ value, and the hydrated tptn complex is low spin up to 400 K. The present crystallographic results, together with previously reported structural results for the tpen complex at two temperatures, are used to show that the conversion from low spin to high spin leads to an increase in the trigonal twist of these distorted octahedral complexes. The influence of this variation in trigonal twist on the rate of $^5T_2 \rightarrow {}^1A_1$ intersystem crossing is examined with variable-temperature laser-flash photolysis. Data collected for the tpen complex in MeOH in the 190−294 K range give a linear Arrhenius plot with an activation energy of $E_a = 767 \pm 22$ cm^{-1} and a preexponential term of $A = (1.35 \pm 0.2) \times 10^9$ s^{-1}. The tppn complex gives similar results of $E_a = 771 \pm 17$ cm^{-1} and $A = (1.45 \pm 0.2) \times 10^9$ s^{-1}. At 294 K the rate (k_{-1}) for the $^5T_2 \rightarrow {}^1A_1$ intersystem crossing is 2.87×10^7 s^{-1} for the tpen complex, and 3.21×10^7 s^{-1} for the tppn complex. On the other hand the tptn complex has $k_{-1} = 6.25 \times 10^8$ s^{-1} at 295 K as measured with a picosecond spectrometer, and together with nanosecond data measured in the 186−210 K range gives an Arrhenius activation energy of $E_a = 777 \pm 50$ cm^{-1} with $A = (2.6 \pm 0.8) \times 10^{10}$ s^{-1}. The bis(tridentate) complex [Fe$(dpa)_2$]$(ClO_4)_2$ in MeOH is found to give $k_{-1} = 4.59 \times 10^7$ s^{-1} at 282 K and with the 191−282 K data gives Arrhenius values of $E_a = 339 \pm 13$ cm^{-1} and $A = (2.5 \pm 0.25) \times 10^8$ s^{-1}. The terpyridine complex [Fe$(terpy)_2$]$(ClO_4)_2$ is found to have $k_{-1} = 1.0 \times 10^8$ s^{-1} in MeOH at 239 K, and the analysis of 190−239 K data gives $E_a = 532 \pm 36$ cm^{-1} and $A = (2.4 \pm 0.4) \times 10^9$ s^{-1}. Previous studies have shown that the greater the trigonal twist, the lower in energy is the $^3T_1$ state which facilitates the spin−orbit interaction between the $^5T_2$ high-spin and $^1A_1$ low-spin states. It is suggested that the trigonal twist is a vibrational coordinate strongly coupled to the $^5T_2 \rightarrow {}^1A_1$ intersystem crossing. It is additionally shown that the data are consistent with a model wherein the "intrinsic" rate of $^5T_2 \rightarrow {}^1A_1$ intersystem crossing, as gauged by the preexponential term, is a function of how far along the reaction coordinate a complex proceeds.

Introduction

The study of excited electronic states in transition metal complexes is a vast area of research.[4] One interesting subset of this field involves intersystem crossing, where a complex converts from one state to another which has a different spin multiplicity. In general, it is not easy to study intersystem crossing, for it involves excited electronic states of molecules. Spin-crossover complexes, which have been studied for several years,[5] are involved in intersystem crossing between the ground electronic state and a thermally populated excited state with a different spin multiplicity. The most thoroughly studied spin-

⊗ Abstract published in *Advance ACS Abstracts,* March 1, 1996.

(1) University of California at San Diego.

(2) Present address: Department of Chemistry, University of California at Berkeley, Berkeley, CA 94720.

(3) University of Delaware.

(4) For general references on inorganic photochemistry, see: (a) Roundhill, D. M. *Photochemistry and Photophysics of Metal Complexes*; Plenum Press: New York, 1994. (b) Ferraudi, G. J. *Elements of Inorganic Photochemistry*, Wiley-Interscience: New York, 1988. (c) *Concepts in Inorganic Photochemistry*; Adamson, A., Fleischauer, P. D., Eds.; Wiley-Interscience: New York, 1975.

(5) (a) Gütlich, P.; Hauser, A.; Spiering, H. *Angew. Chem., Int. Ed. Engl.* **1994**, *33*, 2024. (b) Gütlich, P.; Hauser, A. *Coord. Chem. Rev.* **1990**, *97*, 1−22. (c) Toftlund, H. *Coord. Chem. Rev.* **1989**, *94*, 67. (d) König, E. *Prog. Inorg. Chem.* **1987**, *35*, 527−622. (e) Maeda, Y.; Takashima, Y. *Comments Inorg. Chem.* **1988**, *7*, 41. (f) König, E.; Ritter, G.; Kulshreshtha, S. K. *Chem. Rev.* **1985**, *85*, 219. (g) Gütlich, P. In *Chemical Mössbauer Spectroscopy*; Herber, R. H., Ed.; Plenum Press: New York, 1984. (h) Gütlich, P. *Struct. Bonding (Berlin)* **1981**, *44*, 83. (i) Scheidt, W. R.; Reed, C. A. *Chem. Rev.* **1981**, *81*, 543. (j) Hauser, A. *Comments Inorg. Chem.* **1995**, *17*, 17.

0020-1669/96/1335-2100$12.00/0

crossover complexes are those of Fe^{II}, where the ground state is the low-spin (d^6) $^1A_1$ state with a low-energy high-spin excited $^5T_2$ state. Simply stated the intersystem crossing (in an octahedral Fe^{II} spin-crossover complex) involves an interconversion between low-spin $t_{2g}{}^6$ and high-spin $t_{2g}{}^4e_g{}^2$ configurations. Intersystem crossing in a spin-crossover complex can, thus, be considered as an intramolecular electron transfer.

The rate of spin-state interconversion in spin-crossover complexes is generally quite fast at room temperature. For Fe^{II} spin-crossover complexes, the observed rate constants are typically in the range of 10^7-10^8 s^{-1}. The very first measurement of spin-state interconversion rates for a complex in solution was reported in 1973 by Beattie *et al*.[6] using the laser-Raman temperature-jump technique. For the Fe^{II} spin-crossover complex [$Fe(HB(pz)_3)_2$], where $HB(py)_3^-$ is the hydrotris(pyrazolyl)-borate anion, they observed a relaxation time of 32 ns, which corresponds to interconversion rates of 1×10^7 and 2×10^7 s^{-1} for the $^1A_1 \rightarrow {}^5T_2$ and $^5T_2 \rightarrow {}^1A_1$ processes, respectively. Several years later Beattie also pioneered the use of ultrasonic relaxation,[7] where the observed relaxation time for [$Fe(HB(pz)_3)_2$] of 33.0 ± 0.7 ns is in good agreement with the value obtained from the temperature-jump experiment. A comprehensive study of 14 complexes of Fe^{II}, Fe^{III}, and Co^{II} was reported by Dose *et al*.[8] in 1978 and represented the first detailed study of the kinetics of spin-state interconversion.

A significant breakthrough was achieved in 1982 when McGarvey and Lawthers reported[9] that the kinetics of spin-state interconversion in spin-crossover complexes could be monitored using a laser pulse to excite the sample from one spin state to another. This opened up a variety of possibilities since, with the application of laser photolysis, it is possible to study complexes over a wider range of conditions (*e.g*., temperature, sample state) than was possible with either the temperature-jump or ultrasonic methods. It was through the use of laser photolysis that Xie and Hendrickson[10] reported the observation of temperature-independent kinetics for the $^5T_2 \rightarrow {}^1A_1$ relaxation of a Fe^{II} spin-crossover complex diluted in a polymer film. This provided the first evidence for the occurrence of quantum-mechanical tunneling in spin-crossover complexes. Since this report, other workers[11] have observed temperature-independent rates for $^5T_2 \rightarrow {}^1A_1$ relaxations of Fe^{II} spin-crossover complexes. Recent reviews[5j,12] have summarized the results of the studies of the kinetics of spin-crossover complexes.

The goal of this work was to elucidate in terms of microscopic details the mechanism of spin-state interconversion in spin-crossover and related complexes. The conversion between the low-spin and high-spin states of a Fe^{II} spin-crossover complex can be described in terms of the "one-dimensional" potential-energy diagram shown in Figure 1. The complex can exist in one of two states, and the potential-energy curve for each is represented by a parabola, where the potential energy of the complex is plotted as a function of the reaction coordinate. For a Fe^{II} spin-crossover complex the $^1A_1$ and $^5T_2$ states are vibronically coupled (electronic and vibrational coordinates interact). The reaction coordinate refers to whichever normal vibrational mode or combination of modes is coupled to the spin-state interconversion. The rate at which a Fe^{II} complex converts from the $^1A_1$ to the $^5T_2$ state, or *vice versa*, depends on the magnitude of the change in the reaction coordinate (ΔQ), the zero-point energy difference (ΔE_0), and the resonance energy (H_{ab}) which is also called the tunneling matrix element. The quantity H_{ab} gauges the magnitude of the electronic interaction of the $^1A_1$ and $^5T_2$ states. These two states have a $\Delta S = 2$ difference in spin multiplicities and, consequently interact via a second-order spin−orbit interaction through the intermediacy of a $^3T_1$ state.

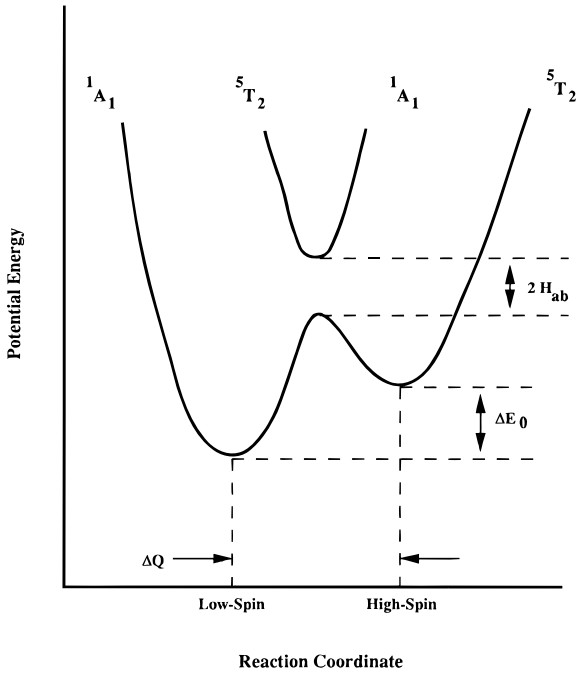

Figure 1. One-dimensional potential-energy diagram for $\Delta S = 2$ spin-crossover transition in a d^6 transition metal complex. See the text for a discussion of the parameters indicated.

To understand the microscopic details of the mechanism of spin-state interconversion, it is necessary to characterize for a given spin-crossover complex not only the values of ΔE_0 and H_{ab}, but most importantly the vibrational modes which make up the reaction coordinate. Since spin-crossover complexes have been known for more than 60 years, it comes as no surprise that there are already opinions in the literature as to what modes are important in the spin-crossover transformation. The single most distinctive characteristic is the change in metal−ligand bond length that accompanies the transformation. For a Fe^{II} spin-crossover complex there are two electrons in the e_g^* σ antibonding orbitals for the $^5T_2$ high-spin state. This results in a marked increase in metal−ligand bond length when an Fe^{II} spin-crossover complex converts from the $^1A_1$ to the $^5T_2$ state. There exists an extensive database[5d,h,13] which shows that the increase in metal−ligand bond distance (Δr) is in the range of 0.15−0.2 Å[14] for Fe^{II} spin-crossover complexes, while Fe^{III} spin-

(6) Beattie, J. K.; Sutin, N.; Turner, D. H.; Flynn, G. W. *J. Am. Chem. Soc*. **1973**, *95*, 2052.
(7) (a) Beattie, J. K.; Binstead, R. A.; West, R. J. *J. Am. Chem. Soc*. **1978**, *100*, 3044. (b) Binstead, R. A.; Beattie, J. K.; Dewey, T. G.; Turner, D. H. *J. Am. Chem. Soc*. **1980**, *102*, 6442.
(8) Dose, E. V.; Hoselton, M. A.; Sutin, N.; Tweedle, M. F.; Wilson, L. J. *J. Am. Chem. Soc*. **1978**, *100*, 1142.
(9) (a) McGarvey, J. J.; Lawthers, I. *J. Chem. Soc., Chem. Commun*. **1982**, 906. (b) Lawthers, I.; McGarvey, J. J. *J. Am. Chem. Soc*. **1984**, *106*, 4280. (c) McGarvey, J. J.; Lawthers, I.; Toftlund, H. *J. Chem. Soc., Chem. Commun*. **1984**, 1576. (d) McGarvey, J. J.; Toftlund, H.; Alobaidi, A. H. R.; Taylor, R. P.; Bell, S. E. J. *Inorg. Chem*. **1993**, *32*, 2469. (e) Alobaidi, A. H. R.; McGarvey, J. J.; Taylor, K. P.; Bell, S. E. J.; Jensen, K. B.; Toftlund, H. *J. Chem. Soc., Chem. Commun*. **1993**, 536.
(10) Xie, C.-L.; Hendrickson, D. N. *J. Am. Chem. Soc*. **1987**, *109*, 6981.
(11) (a) Hauser, A. *Coord. Chem. Rev*. **1991**, *111*, 275, and references cited therein. (b) Hauser, A.; Vef, A.; Adler, P. *J. Chem. Phys*. **1991**, *95*, 8710. (c) Hauser, A. *Chem. Phys. Lett*. **1990**, *173*, 507.
(12) Beattie, J. K. *Adv. Inorg. Chem*. **1988**, *32*, 1.
(13) (a) Martin, R. L.; White, A. H. *Trans. Met. Chem*. **1968**, *4*, 113. (b) Goodwin, H. A. *Coord. Chem. Rev*. **1976**, *18*, 293. (c) Bacci, M. *Coord. Chem. Rev*. **1988**, *86*, 245. (d) König, E. *Struct. Bonding (Berlin)* **1991**, *76*, 51.

crossover complexes tend to show slightly smaller changes with values in the range of $\Delta r \simeq 0.1-0.15$ Å. These observations have prompted most workers in the field to assume that the spin-state interconversion is coupled to the symmetric breathing mode of the complex.

Although changes in the metal−ligand bond length do accompany the spin-crossover transition, this does *not* necessarily mean that the *kinetics* of the process are a reflection of this vibrational mode. The transition state for the spin-crossover spin-state change could occur along a totally different coordinate, implying simply that the observed changes in metal−ligand bond length occur *after* the system has already been established on the new potential-energy surface.

It was the hypothesis of this work that a very strong candidate for the active vibrational coordinate in spin-crossover dynamics is a torsional mode. This idea originates from work by Purcell[15] and Vanquickenborne[16] who independently established a connection between the enantiomerization of d^6 transition metal complexes and spin-state interconversion. Specifically, two torsional coordinates were considered by these authors: a trigonal twist (*i.e.*, Bailar twist) and a rhombic twist (Ray−Dutt twist). The trigonal twist can be described as the motion of the two trigonal faces of an octahedron with respect to each other:

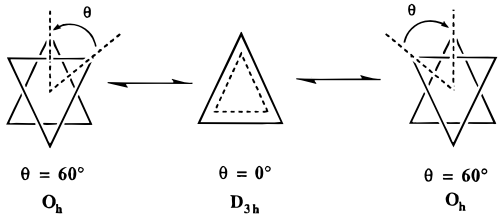

The parameter θ gauges the extent of this distortion relative to a perfect octahedron (O_h, $\theta = 60°$) or a trigonal prismatic structure (D_{3h}, $\theta = 0°$). The trigonal twist therefore occurs about the C_3 axis of the octahedron and reduces the local symmetry to C_{2v} in the intermediate stages of the transformation. The rhombic distortion is more difficult to represent but can be thought of as an analogous distortion about the C_2 axis of the complex. Since all of the conclusions mentioned below concerning state crossings hold equally well for both coordinates, we shall restrict our discussion to the trigonal twist since it is easier to visualize.

Purcell[15] carried out angular overlap calculations in an attempt to rationalize both the unusually fast rate of enantiomerization in $[Fe(phen)_3]^{2+}$ and to place on theoretical grounds the hypothesis[17] that *cis*-$[Fe(phen)_2(NCBPh_3)_2]$ exhibits synchronous enantiomerization and spin-state interconversion in CH_2Cl_2. The angular overlap calculations showed that distortion along purely torsional coordinates results in a crossing of the singlet and quintet surfaces. Using his model, Purcell was able to reproduce quite well the experimental value for the rate of enantiomerization in $[Fe(phen)_3]^{2+}$. A torsional mode is highly attractive from the standpoint of a transition state in a classical description of spin-state interconversion. These normal models are characterized by relatively low energies (<100 cm^{-1}) and hence would result in low-energy transition states relative to those produced along bond-stretching coordinates ($\hbar\omega \simeq 300$ cm^{-1}). In addition, according to Purcell's calculation torsional modes cause a *significant net stabilization* of $S = 1$ states relative to *both* the low-spin and high-spin states. This will result in a significant increase in H_{ab} and therefore enhance the rate of spin-state interconversion by further stabilizing the transition state. The results of Purcell[15] and Vanquickenborne[16] strongly suggest that enantiomerization in d^6 complexes occurs via a spin-crossover transformation. In the present work we approach the problem in the opposite sense and postulate that the molecular mechanism for spin-state interconversion involves coupling to a torsional vibration of the spin-crossover complex.

Finally, it is relevant to note that Endicott and co-workers[18] presented results including those from molecular mechanics calculations to explain the range of ^2E excited state lifetimes observed for Cr^{III} complexes. They concluded that the greater the tendency of the ligand to twist along a trigonal coordinate, the shorter the lifetime of the ^2E excited state is for a Cr^{III} complex. Large-amplitude trigonal distortions facilitate the spin-forbidden $^2E \rightarrow {}^4A_2$ relaxation.

In this first paper a series of structurally related Fe^{II} complexes are characterized by X-ray structural and susceptibility data. There is an attempt to correlate the flexibilities of the ligands in the series with the activation energies for $^5T_2 \rightarrow {}^1A_1$ relaxation measured by means of nanosecond laser flash photolysis. In a future paper the variable-temperature kinetic data for the $^5T_2 \rightarrow {}^1A_1$ relaxation in the series of Fe^{II} complexes are fit to three different theories of electron transfer. This is done in an effort to determine the nature of the vibrational mode(s) which is (are) coupled to the $^5T_2 \rightarrow {}^1A_1$ spin-crossover transition.

Experimental Section

All materials were of reagent grade and used without further purification unless otherwise indicated. All synthetic procedures involving Fe^{II} complexes were carried out in thoroughly deoxygenated solvents under an inert atmosphere of either N_2 or Ar using standard Schlenk techniques unless otherwise indicated. All chemicals and solvents were purchased from either Fischer or Aldrich. The synthesis of $[Fe(t\text{-tpchxn})](ClO_4)_2$ (*t*-tpchxn = *trans*-1,2-diaminocyclohexane) is described in the literature.[19]

Compound Preparations. *N,N,N′,N′*-Tetrakis(2-pyridylmethyl)-1,2-ethylenediamine (tpen). This compound was prepared as previously reported.[20]

***N,N,N′,N′*-Tetrakis(2-pyridylmethyl)-1,2-propylenediamine (tppn).** This compound was prepared by a modification of a previously reported procedure.[21] Approximately 4.8 mL (50 mmol) of 2-pyridinecarboxaldehyde was dissolved in 20 mL of EtOH. To this solution was added 2.1 mL (25 mmol) of 1,2-propylenediamine in a dropwise fashion, resulting in the immediate formation of a clear, yellow solution. The solution was gently heated for 1 h and then allowed to cool. To this now amber solution was added ∼2.5 g of $NaBH_4$ *in small portions* so that gas evolution was not too excessive. This opaque, pale-orange solution was stirred overnight. The resulting thick, yellow emulsion was heated to reflux for 1 h and allowed to cool. Slow addition of ∼7 mL of concentrated HCl resulted in dissipation of the emulsion, giving a milky-orange mixture. This solution was stirred for approximately 1 h, after which the solution was made slightly basic with aqueous

(14) In the case of $Fe(dppen)_2Cl_2 \cdot 2(CH_3)CO$ the F−P bond length increases by as much as $\Delta r = 0.28$ Å; see: Cecconi, F.; DiVaira, M.; Midollini, S.; Orlandini, A.; Sacconi, L. *Inorg. Chem.* **1981**, *20*, 3423.
(15) Purcell, K. F. *J. Am. Chem. Soc.* **1979**, *101*, 5147.
(16) Vanquickenborne, L. G.; Pierloot, K. *Inorg. Chem.* **1981**, *20*, 3673.
(17) Purcell, K. F.; Zapata, J. P. *J. Chem. Soc., Chem. Commun.* **1978**, 497.
(18) (a) Perkovic, M. W.; Heeg, M. J.; Endicott, J. F. *Inorg. Chem.* **1991**, *30*, 3140. (b) Endicott, J. F.; Ramasami, T.; Tamilarasan, R.; Lessard, R.; Ryu, C. K.; Brubaker, G. R. *Coord. Chem. Rev.* **1987**, *77*, 1. (c) Lessard, R. B.; Endicott, J. F.; Perkovic, M. W.; Ochromowycz, L. M. *Inorg. Chem.* **1989**, *28*, 2574. (d) Lessard, R. B.; Heeg, M. J.; Buranda, T.; Perkovic, M. W.; Schwarz, C. L.; Rudong, Y.; Endicott, J. F. *Inorg. Chem.* **1992**, *31*, 3091.
(19) McCusker, J. K.; Toftlund, H.; Rheingold, A. L.; Hendrickson, D. N. *J. Am. Chem. Soc.* **1993**, *115*, 1797.
(20) Chang, H.-R.; McCusker, J. K.; Toftlund, H.; Wilson, S. R.; Trautwein, A. X.; Winkler, H.; Hendrickson, D. N. *J. Am. Chem. Soc.* **1990**, *112*, 6814.
(21) Toftlund, H.; Yde-Andersen, S. *Acta Chem. Scand.* **1981**, *A35*, 575.

NaOH. A white precipitate was filtered off, and the filtrate was concentrated to a volume of 5 mL. This concentrate was extracted with five 40 mL portions of $CHCl_3$, and the extract was dried with $MgSO_4$. This clear, pale-yellow solution was concentrated and the residue redissolved in 20 mL of EtOH. To this stirred solution was added 8.0 g (63 mmol) of 2-picolylchloride hydrochloride in small portions to allow for dissolution. The reaction mixture was made slightly basic with aqueous NaOH (to pH $\simeq$ 8.5), resulting in a somewhat biphasic, red reaction mixture. The reaction was allowed to stir for 3 days, during which time the pH was maintained between 7 and 9 by dropwise addition of aqueous NaOH. The reaction mixture was filtered, yielding a pink solid and a deep red filtrate. The solid was washed with cold H_2O, which dissipated some of the pink hue, and dried *in vacuo*. The ligand is isolated with one molecule of hydration. The yield was 18%. Anal. Calcd for $C_{27}H_{32}N_6O$: C, 71.03; H, 7.06; N, 18.41. Found: C, 71.07; H, 6.72; N, 18.08.

***N,N,N′,N′*-Tetrakis(2-pyridylmethyl)-1,3-propylenediamine (tptn).** This compound was prepared analogously to tppn using 1,3-propylenediamine instead of 1,2-propylenediamine. The yield for this reaction was <10%. Anal. Calcd for $C_{27}H_{30}N_6$: C, 73.94; H, 6.89; N, 19.16. Found: C, 73.77; H, 6.95; N, 19.00.

Bis(2-pyridylmethyl)amine (dpa). This ligand was graciously provided by Professor Robert Buchanan of the University of Louisville as a 3HCl salt and prepared according to a previously reported method.[22] To isolate the free base, approximately 0.5 g of dpa·3HCl was dissolved in 5 mL of H_2O. To this stirred solution was added an aqueous solution of Na_2CO_3 (1 g in 15 mL of H_2O) in a dropwise fashion until gas evolution ceased. This solution was extracted with seven 50 mL portions of CH_2Cl_2, and the extract was dried over $MgSO_4$. The CH_2Cl_2 solution was evaporated to dryness, leaving an oily residue. This residue was redissolved in 15 mL of MeOH for reaction with $FeCl_2$ (*vide infra*).

$FeCl_2 \cdot 2H_2O$. A 25 g amount of $FeCl_2 \cdot 4H_2O$ was dissolved in deoxygenated H_2O and mixed with 1 mL of concentrated HCl and 1 g of Fe powder. The solution was heated in an oil bath under an N_2 atmosphere for 30 min. The solution was filtered while warm, and the pale-green filtrate was evaporated to dryness, leaving a pale green-white solid. White $FeCl_2 \cdot 2H_2O$ was obtained upon heating this solid under a hard vacuum at 80 °C for 1 h. This purified ferrous chloride was stored under N_2 and used as needed.

[Fe(tpen)](ClO$_4$)$_2 \cdot {}^2/_3$H$_2$O. This compound was prepared as previously described.[20]

[Fe(tppn)](ClO$_4$)$_2$. Approximately 0.091 g (0.56 mmol) of $FeCl_2 \cdot 2H_2O$ was dissolved in 10 mL of deoxygenated 1:1 MeOH/H_2O and heated to 50 °C. To this stirred solution was added 0.23 g (0.52 mmol) of tppn in 5 mL of deoxygenated 1:1 MeOH/H_2O, resulting in the immediate formation of a clear, red solution. This solution was stirred at 50 °C for approximately 2 h. The heat was removed, and to the warm, stirred solution was added a solution of $NaClO_4$ (*ca*. 0.3 g in 8 mL of H_2O) in a dropwise fashion. The reaction mixture was allowed to cool to room temperature and then immersed in ice. Scratching induced the formation of a brownish-red, microcrystalline precipitate. The solid was filtered, washed with small portions of cold H_2O, and dried *in vacuo*. The compound is isolated as a monohydrate and is stable in air as a solid. Solutions of the compound are also reasonably stable for several days in air (soluble in H_2O, MeOH, acetone, and MeCN), but it is recommended that care be taken to exclude air in making up solutions for spectroscopic work. Anal. Calcd for $FeC_{27}H_{32}N_6O_9Cl_2$: C, 45.59; H, 4.53; N, 11.81; Fe, 7.85; Cl, 10.03. Found: C, 45.89; H, 4.46; N, 11.81; Fe, 7.98; Cl, 10.08.

[Fe(tptn)](ClO$_4$)$_2$. This compound was prepared analogously to [Fe(tppn)](ClO$_4$)$_2$ using $FeCl_2$ and tptn and is isolated as a partial hydrate. The compound is very stable as a solid and is reasonably stable in solution, showing no signs of significant decomposition upon standing in air for several days. Anal. Calcd for $FeC_{27}H_{31}N_6O_{8.5}Cl_2$: C, 46.18; H, 4.30; N, 11.97; Fe, 7.96. Found: C, 45.92; H, 4.07; N, 12.03; Fe, 8.00.

[Fe(dpa)$_2$](ClO$_4$)$_2$. A quantity of 0.13 g (0.80 mmol) of $FeCl_2 \cdot 2H_2O$ was dissolved in 2−3 mL of deoxygenated H_2O and added to a stirred deoxygenated MeOH solution of dpa (*vide supra*), resulting in the immediate formation of a clear, deep red solution. This solution was heated to *ca*. 50 °C for a period of 2 h, after which time the heat was removed and an aqueous solution of $NaClO_4$ (0.2 g in 3 mL of H_2O) was added in a dropwise fashion. The solution was allowed to cool, and N_2 was passed over the top of the solution to slowly evaporate the solvent. A microcrystalline product formed after 1 day and was isolated by filtration as a monohydrate. The compound is stable in air as a solid but decomposes in solutions exposed to air upon standing for several hours. Anal. Calcd for $FeC_{24}H_{28}N_6O_9Cl_2$: C, 42.94; H, 4.20; N, 12.52; Fe, 8.55. Found: C, 43.13; H, 3.86; N, 12.20; Fe, 8.70.

[Fe(bpy)$_3$](ClO$_4$)$_2$. Approximately 0.95 g (6.0 mmol) of 2,2′-bipyridine (bpy) was dissolved in 20 mL of MeOH. This solution was then pumped and purged with N_2. To the stirred solution was added 0.34 g (2.0 mmol in 5 mL H_2O) of $FeCl_2 \cdot 2H_2O$, resulting in the immediate formation of a clear, blood-red solution. This reaction mixture was gently heated and stirred for *ca*. 1 h and allowed to cool to room temperature. Dropwise addition of an aqueous solution of $NaClO_4$ (0.5 g in 5 mL of H_2O) resulted in the immediate formation of a red, microcrystalline precipitate. The solid was filtered and dried *in vacuo* for 24 h. The optical spectrum of the compound was identical with that reported in the literature.[23]

[Fe(phen)$_3$](ClO$_4$)$_2$. This compound was prepared analogously to [Fe(bpy)$_3$](ClO$_4$)$_2$ using 1,10-phenanthroline (phen) instead of bpy. The deep red, microcrystalline product was isolated by filtration and dried *in vacuo*.

[Fe(terpy)$_2$](ClO$_4$)$_2$. A 0.16 g (1.0 mmol) amount of $FeCl_2 \cdot 2H_2O$ was dissolved in 8 mL of deoxygenated H_2O and added to a stirred MeOH solution containing 0.47 g (2.0 mmol) of 2,2′,6′,2″-terpyridine (terpy), resulting in the formation of a clear, deep purple solution. The reaction mixture was gently heated to 50 °C for 1 h. To the warm solution was added a solution of $NaClO_4$ (0.25 g in 10 mL of H_2O) in a dropwise fashion. This resulted in the immediate formation of a purple, microcrystalline product that was isolated by filtration and dried *in vacuo*. As with the two previous compounds, identification of the desired product was made by comparison of its optical spectrum with that of an authentic sample.

[Fe(mtpen)](ClO$_4$)$_2$. This compound was prepared according to a previously reported procedure.[21] The compound is identical to [Fe(tpen)](ClO$_4$)$_2$ with the exception that a methyl group is located at the 6-position of one of the pyridine rings. Crystals suitable for X-ray diffraction were obtained by redissolving the sample in 1:1 MeOH/H_2O under N_2 and allowing the solvent to slowly evaporate over a period of several days.

Physical Measurements. Magnetic Susceptibility. Magnetic susceptibility data were collected on a VTS-50 Series 800 SQUID susceptometer (S.H.E. Corp.) interfaced to an Apple II+ computer. The sample was packed in a cylindrical Delrin sample container with an inner diameter of approximately 4 mm. Sample temperature control was achieved using a S.H.E. digital temperature device. Each data point was taken as the average of five samplings after the sample had reached thermal equilibrium. A magnetic field of 10.0 kG was used. For all of the data reported, diamagnetic corrections estimated from Pascal's constants were applied in determining the molar paramagnetic susceptibility of the compound.

Electronic Absorption Spectra. Variable-temperature electronic absorption spectra were recorded on a Hewlett-Packard Model 8452A diode array spectrophotometer. Temperature control was achieved using a Hewlett-Packard Model 89054A thermostated cell holder, connected to a Fisher Scientific Model 800 Isotemp circulating bath. Temperature stability was better than $\pm$0.3 K; the absolute accuracy is estimated at $\pm$1 K. Measurements were carried out in spectrophotometric-grade solvents. Each spectrum represents a signal average of 250 individual spectra taken at 0.1 s interals after the solution had equilibrated for 15 min. All spectral changes were found to be reversible unless otherwise indicated.

X-ray Structure of [Fe(mtpen)](ClO$_4$)$_2 \cdot {}^2/_3$H$_2$O. The structure for this compound was solved in the Department of Chemistry at the University of California at San Diego. The structure was solved at two temperatures, 173 and 296 K; the former structure was determined

(22) Gruenwedel, D. W. *Inorg. Chem.* **1968**, *7*, 495.

(23) Palmer, R. A.; Piper, T. S. *Inorg. Chem.* **1966**, *5*, 864.

Table 1. Crystallographic Data for [Fe(mtpen)]$(ClO_4)_2 \cdot {}^2/_3H_2O$

	173 K	296 K
formula	$C_{27}H_{31.33}N_6O_{8.67}Cl_2Fe$	$C_{27}H_{31.33}N_6O_{8.67}Cl_2Fe$
fw, g/mol	705.3	705.3
color, habit	brown, prismatic	brown, prismatic
cryst dimens, mm	0.11 × 0.18 × 0.36	0.11 × 0.18 × 0.36
cryst syst	monoclinic	monoclinic
space group	*C*2/*c*	*C*2/*c*
cell dimens		
a, Å	41.390(13)	41.891(13)
b, Å	9.5239(16)	9.5823(16)
c, Å	24.016(6)	24.224(6)
β, deg	108.24(3)	108.53(3)
V, Å^3	8991(4)	9220(4)
Z (molecules/cell)	12	12
D(calcd), g/cm^3	1.563	1.524
D(measd), g/cm^3		1.49(5)
abs coeff, mm^{-1}	0.741	0.723
radiation type	Mo Kα (λ = 0.710 73 Å)	Mo Kα (λ = 0.710 73 Å)
goodness of fit (*S*)[a]	2.23	2.19
2θ range, deg	3.0° ≥ 2θ ≤ 45.0°	4.0° ≤ 2.θ ≤ 45.0°
total data	6356	6537
unique data	5840	6016
obsd data	2844	2784
R,[b] %	7.50	8.11
R_w,[c] %	7.60	8.09

[a] $S = [\sum w(|F_o| - F_c|)^2(m - n)]^{1/2}$. [b] $R = \sum||F_o| - F_o||/\sum|F_o|$. [c] $R_w = [\sum w(|F_o| - |F_c|)^2/\sum w|F_o|^2]^{1/2}$.

in an attempt to improve the *R*-factor from the structure at 296 K due to disorder in the ClO_4^- anions (*vide infra*). The details for both structures are virtually identical. Systematic absences indicated the space group to be either *C*2/c or *Cc*. The centrosymmetric model was chosen because $\langle E^2 - 1\rangle$ was 0.960 and because the noncentrosymmetric model would require the asymmetric unit to contain three independent molecules for which there was insufficient data. With $Z = 12$ in *C*2/*c* there is one cation present on a general position and one on a 2-fold rotation axis. This requires that the methyl group is statistically disordered. It was discovered that the disorder in the position of the pyridine ring containing the methyl group was present for both the general position and special position cations.

The ClO_4^- ions were observed to be undergoing large-amplitude librational motions at 286 K; these librations were significantly reduced at 173 K. The low-temperature structure with all Fe, Cl, N, and C(1)−C(9) atoms refined anisotropically gave $R = 0.0945$ and $R_w = 0.0989$. Anisotropic refinement of the oxygen atoms of the perchlorate ions and the water solvate led to convergence after four cycles with $R = 0.0750$ and $R_w = 0.0760$. Due to our inability to uniquely locate the water hydrogen atoms, it is impossible to make definitive statements concerning hydrogen-bonding contacts. However, O(w)···O(2) and O(w)···O(12′) distances are 3.30 and 3.07 Å, respectively. Pertinent crystallographic details for the structures at both temperatures are given in Table 1.

X-ray Structure of [Fe(tppn)]$(ClO_4)_2 \cdot H_2O$. The structure of this complex was determined at the University of Delaware. Crystallographic data on this compound are collected in Table 2. All specimens tested diffracted weakly and broadly due to the presence of loosely bound and fractionally missing water molecules as well as ambiguously located ClO_4^- ions. Photographic characterization showed 2/*m* Laue symmetry, and systematic absences in the diffraction data unambiguously identified the space group as $P2_1/n$. The upper limit of 2θ for available data was restricted by the diffuseness of diffraction. Correction for absorption effects was done by semiempirical methods.

The structure was solved by direct methods and a series of difference Fourier syntheses. For each complex cation a molecule of H_2O loosely hydrogen-bonded to both ClO_4^- counterions was found in the crystal lattice. Refinement of the site occupancy of the water-molecule oxygen atom O(9) [final value = 0.73(3)] suggests partial solvent loss, although we have chosen to continue to formulate the compound as a monohydrate.

Table 2. Crystallographic Data for [Fe(tppn)]$(ClO_4)_2 \cdot H_2O$

formula	$C_{27}H_{31}N_6O_9Cl_2Fe$
fw, g/mol	710.33
color, habit	red, plates
cryst dimens, mm	0.05 × 0.32 × 0.32
cryst syst	monoclinic
space group	$P2_1/n$
temp, K	296
cell dimens	
a, Å	12.979(4)
b, Å	12.624(4)
c, Å	19.475(6)
β, deg	108.17(2)
V, Å^3	3031.9(18)
Z (molecules/cell)	4
D(calcd) g/cm^3	1.556
abs coeff, mm^{-1}	0.730
radiation type	Mo Kα (λ = 0.710 73 Å)
goodness of fit (*S*)[a]	1.550
2θ range, deg	4.0° ≤ 2θ ≤ 45.0°
total data	4311
unique data	3952
obsd data	2357
R,[b] %	11.98
R_w,[c] %	11.41

[a] $S = [\sum w(|F_o| - F_c|)^2(m - n)]^{1/2}$. [b] $R = \sum||F_o| - F_o||/\sum|F_o|$. [c] $R_w = [\sum w(|F_o| - |F_c|)^2/\sum w|F_o|^2]^{1/2}$.

All non-hydrogen atoms except for the water-molecule oxygen atom were refined anisotropically. Hydrogen atoms were placed in idealized locations. The ClO_4^- ions were fixed as rigid tetrahedrons with a common refined Cl−O distance [final value = 1.355(4) Å]. All computations used SHELXTL (5.1) software (G. Sheldrick, Nicolet, Madison, WI).

Nanosecond Laser Photolysis Experiments. A nanosecond time-resolved laser photolysis apparatus was constructed where the centerpiece of the system is a Lambda-Physik LPX 205iC rare-gas excimer laser configured for XeCl. The laser was operated in single-shot mode at a pressure of ∼3.3 atm with 22.0 kV electrical discharge to produce a ∼28 ns pulse at 308 nm. This pulse was directed into a Lambda-Physik Model FL3002 dye laser. The dye used for all of the experiments on the tpen series of complexes was Coumarin 120 (Lambdachrome) dissolved in MeOH, which allowed for tunable excitation in the range of 418−460 nm. The output pulse from the dye laser was measured by diffuse scattering into a R1547 photomultiplier tube (Hamamatsu) to be 24 ± 1 ns. The dye output was passed through a spatial filter, and a portion of the beam (∼4%) was split off and directed into a power meter (Scientech Mentor MD10 energy meter with a Model MC2505 volume absorbing disk calorimeter) for monitoring pulse energies during the experiment. The beam was directed at the sample through a fixed 2.0 mm aperture using an enhanced Al mirror (Melles Griot) to yield a fairly uniform excitation source without the need for additional focusing. This second aperture in addition to eliminating ASE on the fringes of the laser pulse also greatly reduced backscatter of laser light off of the mirror due to reflections from within the sample chamber of the optical dewar (*vide infra*).

The probe beam consists of a high-energy Xe flash lamp (EG&G Model FX193) operated at variable applied voltages with a pulse duration of ∼2 μs fwhm (full width at half-maximum). In order to avoid unnecessary scattered light from the highly divergent Xe source, an aspheric condenser lens (f_o = 29 mm) was placed directly in front of the Xe lamp to collect better than 95% of the output light intensity. In addition to dramatically attenuating scattered light, this configuration also provided for a nearly parallel-ray light source for focusing onto the sample. The probe beam was focused using a plano-convex lens onto a fixed 2.0 mm aperture to ensure effective overlap with the laser excitation pulse. The clean pulse from the filter was focused onto the sample using matched achromatic lenses. The alignment of the laser beam was such that intersection of the pump and probe beams occurred at *ca*. 90° in the front one-third of the 10 mm cell. After being passed through the sample, the probe beam was then focused onto the 2.0 mm entrance slit of a monochromater (Instruments SA Model H20, f_o

= 200 mm) using a pair of matched achromatic lenses and an aplanatic meniscus lens included to ensure that the $f_o/\phi = 4.2$ of the monochromater was approximately matched by the probe beam. The holographic grating of the monochromater (1200 blaze) was tuned to 414 nm where most of the tpen series molecules were monitored. A S11 photomultiplier tube (PMT) modified slightly in the first few dynode stages for the high intensity of the flash lamp was coupled directly to the end of the monochromater and operated at an applied voltage of −800 V (dc). The ouput from the PMT was terminated through a 50 Ω resistor and monitored in real time using a Tektronix 7912AD digitizing oscilloscope, and the data were collected and transferred to disk using a Tetronix PEP 301 controller (AT386 computer) and the TekMAP driver software. Synchronization of the probe beam, the oscilloscope, and the excimer laser were effected using an electronic timing circuit of local design. All of the data presented represent a signal average of 10 transients, and the data were analyzed using programs of local origin.

The S11 tube as configured for our experiments has a relatively large transit-time spread and is the temporal limitation of the apparatus. The instrument response function (IRF) of the system is 38 ± 2 ns fwhm as measured by diffuse scattering of the laser source. However, the high degree of reproducibility of the IRF enabled us to analyze our data via integral deconvolution (more specifically, iterative reconvolution), which extends our time resolution to below 10 ns. The increased transit-time spread therefore yields an advantage in this particular case. For ordinary room-temperature measurements, the sample was placed in a 10 mm path length optical cuvette and positioned using a home-built sample holder. For variable-temperature measurements, the sample was placed in locally-fashioned thick-walled cuvettes (wall diameter ∼ 1 mm) to guard against cracking of the cell due to thermal cycling. No problems of this kind were experienced using these cells, which were also equipped with a top suitable for sealing the cuvette with a septum. The drawback to the thick-walled cuvettes is that the glass is not of opitcal quality. This resulted in somewhat smaller signal intensities as compared to the optical cells due to necessary repositioning of the pump and probe beams, but did not significantly affect data collection. Experiments were performed by placing the sample cell in a Janis Model 8DT-SVT-OPT dewar equipped with optical windows. This dewar enables measurements to be made between 1.8 and 300 K. A typical data set ran from 190 to 300 K since we were interested in dynamics in fluid media. The use of a 9:1 MeOH/EtOH mixture allowed us in one instance to measure kinetics in solution down to 160 K. Scattering off of the polished Al surfaces inside the dewar cavity is a significant problem with these variable-temperature experiments. It can be reduced to an acceptable level by repositioning the pump beam, using the second spatial filter mentioned above to reduced backscatter off of the mirror, and tuning the probe wavelength away from the laser line (∼10 nm is usually sufficient). However, *care must be exercised in ensuring that scattering is not a significant portion of the observed signal*.

Temperature control was achieved using a LakeShore Model DST-80D temperature controller and a DT-470-SD-13 silicon diode (LakeShore). This factory-installed diode was located below the sample region; we installed a second diode (DT-500-DRC) to monitor the temperature at a position approximately equidistant above the sample region and took the average of the readings on the two diodes as the temperature for the sample. The dewar was operated in the conduction mode with liquid N_2 in the outer chamber and He as the carrier gas into the sample region. A substantial temperature gradient was found across the sample region, particularly at high temperatures (*e.g.*, $\Delta T =$ 7 K at 280 K); this is likely due to the low heat capacity of He gas. Equilibration of the control diode usually occurred within 10 min following a 10° rise in temperature. However, data were only collected once the *monitor* diode had stabilized. At higher temperatures this took in excess of $1-1^1/_2$ h for He flow rates of 2−3 cm^3/min. Higher flow rates did speed up the process but tended to show larger gradients at a given temperature. Because of this gradient problem, measurements were typically only made up to 280 K inside the dewar, with the final point taken outside the dewar at ambient temperature.

Picosecond Laser Photolysis Experiments. For a couple of the systems we examined, the relaxation rate was too fast for our nanosecond apparatus. In these instances we used a picosecond spectrometer in the laboratories of Professor John Simon at the University of California at San Diego. A description of this apparatus is given in the literature.[24] This spectrometer has a ∼80 ps pulse width with excitation available at both 532 and 355 nm. The probe beam originates from a dye laser, and the temporal resolution comes from an optical delay line rather than the real-time measurement characteristic of our nanosecond experiment. The apparatus is capable of delays out to ∼3 ns, which nearly overlaps with our deconvolution analysis. Data from the picosecond spectrometer were also fit by deconvolution of the instrument response function, giving a temporal resolution of ∼50 ps.

Results and Discussion

Compound Preparation and Basic Characterization. It was desirable to have a series of Fe^{II} spin-crossover complexes where the hexadentate ligand is changed such that there would be a variation in the trigonal-twist angle θ (*vide supra*). The ligands should be virtually identical with respect to σ-donor/π-acceptor characteristics so that focus can be directed on the geometric effects on the spin-state interconversion rate. Following the work of Toftlund and co-wokers,[5c,21] Fe^{II} complexes were prepared for the following ligands:

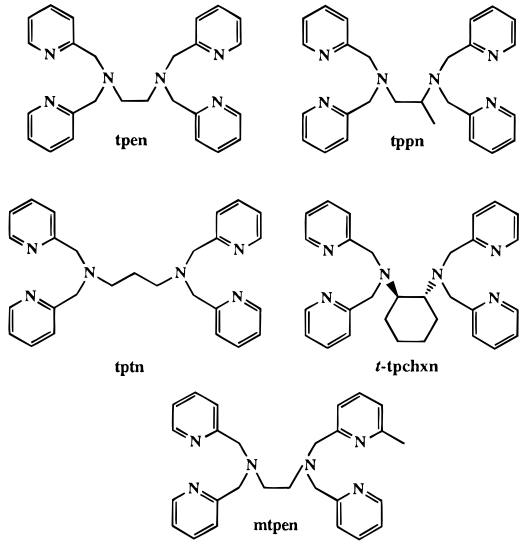

All of these ligands bind to Fe^{II} in a hexadentate fashion which should ensure that the Fe^{II} complexes will be very stable with respect to ligand dissociation (formation constants are $\simeq 10^{25}$; cf. ref 21).

In a previous paper[20] we reported the X-ray structures, ^{57}Fe Mössbauer and magnetic susceptibilities of $[Fe(tpen)](ClO_4)_2$ and the hydrated form $[Fe(tpen)](ClO_4)_2 \cdot {}^2/_3H_2O$. For polycrystalline samples both of these tpen complexes are spin-crossover, where the $T_{1/2}$ temperatures (50% high spin and 50% low spin) were found to be 369 K for the hydrate salt and >400 K for the anhydrous salt.

In another recent paper[19] we reported the X-ray structure and other characteristics of $[Fe(t\text{-tpchxn})](ClO_4)_2$. At room temperature a polycrystalline sample is mostly low spin. Toftlund has reported[25] that in solution the spin equilibrium for this complex is solvent dependent with $T_{1/2} \simeq 365$ K (DMF) and $T_{1/2} \simeq 340$ K (CH_3CN). In our paper[19] we also reported the results of a variable-temperature solution-phase laser photolysis study of a CH_3OH solution of the *t*-tpchxn complex. Biphasic $^1A_1 \leftarrow {}^5T_2$ relaxation kinetics were observed.

The tpen series is particularly attractive for our study because of the manner in which each member of the series is related.

(24) Xie, X.; Simon, J. D. *Opt. Commun.* **1989**, *69*, 303.
(25) McGarvey, J. J.; Lawthers, I.; Heremans, K.; Toftlund, H. *Inorg. Chem.* **1990**, *29*, 252.

The working hypothesis is that low-frequency torsional modes—in particular trigonal twists and/or rhombic distortions—are coupled to the spin-state interconversion. What would be useful in order to experimentally test our hypothesis is a series of ligands designed about a particular reaction coordinate, namely, a torsional mode. This is precisely what is afforded by the tpen series:

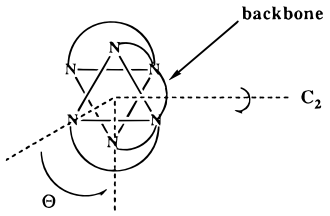

It can be seen that the aliphatic backbone of the hexadentate ligand bridges between the two trigonal faces of the octahedron, spanning in the pseudo-C_2 axis of the molecule. The ligand system is ideally set up for distortion about the C_3 axis while maintaining pseudo-C_2 symmetry throughout. The variation across the ligand series amounts to changing the structure of this backbone from a five-membered ring (tpen and tppn) to a six-membered ring (tptn) to a five-membered ring with a fused-ring bridge (*t*-tpchxn), while leaving all other aspects of the structure relatively unperturbed. In this context another ligand—dpa (dipyridylmethylamine)—is of interest:

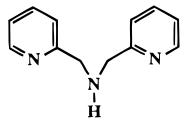

dpa

The structure of the complex when the ligand binds facially to the metal center corresponds to cleavage of the C−C backbone of the hexadentate ligand, allowing for free rotation of the two trigonal faces with respect to each other. Thus, the tpen series allows us to probe the torsional reaction coordinate by varying the flexibility of the molecule from completely free (dpa) to strongly hindered (*t*-tpchxn) without making significant changes in other aspects of the system.

X-ray Crystal Structure of [Fe(mtpen)](ClO$_4$)$_2$·$^2/_3$H$_2$O. The X-ray structure of [Fe(tpen)](ClO$_4$)$_2$·$^2/_3$H$_2$O was reported[20] at 298 and 358 K. At the lower temperature this complex is all low spin, whereas at 358 K it is ∼40% high spin. A higher temperature X-ray structure of this tpen complex is not possible, because it is a perchlorate salt. However, if a methyl substituent is added at the 6-position of one of the pyridyl rings, Toftlund[21] has shown that this complex is high spin at even very low temperatures. Thus, we can use the structure of [Fe(mtpen)](ClO$_4$)$_2$ as a reasonable analogue of the high-spin form of [Fe(tpen)](ClO$_4$)$_2$·$^2/_3$H$_2$O. The structure of the mtpen complex was determined at 173 and 296 K (see Table 1 for details); we shall consider here only the data from the 173 K structure, for at 296 K the complex is still high spin and relative to the 173 K structure there are only small changes (*e.g.*, 0.01−0.02 Å in bond lengths and <0.5° in bond angles).

A drawing of a portion of the unit cell of [Fe(mtpen)](ClO$_4$)$_2$·$^2/_3$H$_2$O at 173 K is shown in Figure 2. This compound crystallizes in the monoclinic space group *C*2/*c* and is isostructural to that of [Fe(tpen)](ClO$_4$)$_2$·$^2/_3$H$_2$O, where there is a fractional occupancy of H$_2$O solvent molecules. Although this may not be too surprising based on the similarities between the two compounds, the fact that $Z = 12$ for [Fe(mtpen)](ClO$_4$)$_2$·$^2/_3$H$_2$O is unusual in that this gives an asymmetric unit containing one complete cation and one cation lying on a 2-fold rotation axis. Since [Fe(mtpen)]$^{2+}$ does not have a 2-fold axis, this observation implies that the pyridyl ring with the 6-methyl substitutent must be disordered throughout the lattice. Refinement of structure was therefore done for both the general position and special position cations with 50% occupancy of the 6-methyl group about the pseudo-2-fold axis that bisects the ethylene backbone of the molecule.

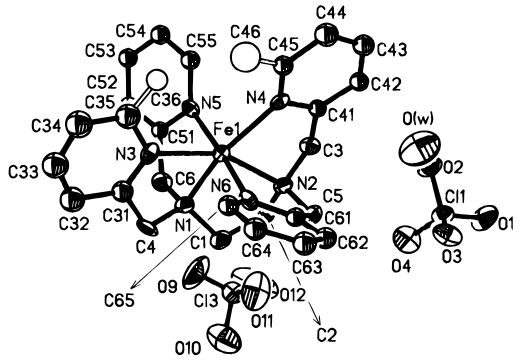

Figure 2. ORTEP drawing of a portion of the unit cell for [Fe(mtpen)](ClO$_4$)$_2$·$^2/_3$H$_2$O. The open circles for C(36) and C(46) indicate 50% occupancies for the disordered 6-methyl group of the pyridine ring.

Table 3. Comparison of Selected Bond Distances and Angles of [Fe(mtpen)](ClO$_4$)$_2$·$^2/_3$H$_2$O with Those of the Anhydrous and Hydrated Forms of [Fe(tpen)](ClO$_4$)$_2$[a]

Distances (Å)

			tpen·$^2/_3$H$_2$O[d]	
	mtpen·$^2/_3$H$_2$O[b]	tpen[c]	298 K	358 K
Fe(1)−N(1)	2.157(12)	2.002(4)	2.022(8)	2.09(1)
Fe(1)−N(2)	2.180(8)	1.996(4)	2.044(8)	2.09(1)
Fe(1)−N(3)	2.121(9)	1.984(4)	2.020(8)	2.07(1)
Fe(1)−N(4)	2.172(11)	1.987(4)	1.977(8)	2.01(1)
Fe(1)−N(5)	2.134(9)	1.990(4)	2.046(8)	2.12(1)
Fe(1)−N(6)	2.156(10)	1.990(4)	2.005(8)	2.03(1)
Fe(2)−N(7)	2.124(8)		2.018(9)	2.09(1)
Fe(2)−N(8)	2.136(13)		1.996(7)	2.06(1)
Fe(2)−N(9)	2.164(10)		1.967(8)	2.01(1)

Angles (deg)

			tpen·$^2/_3$H$_2$O[d]	
	mtpen·$^2/_3$H$_2$O[b]	tpen[c]	298 K	358 K
N(1)−Fe(1)−N(2)	81.3(4)	86.4(2)	85.7(3)	83.6(5)
N(1)−Fe(1)−N(3)	78.2(4)	81.0(2)	82.0(3)	81.0(5)
N(1)−Fe(1)−N(4)	153.5(4)	166.8(2)	164.4(3)	160.9(5)
N(1)−Fe(1)−N(5)	79.4(4)	84.0(2)	83.2(3)	81.4(5)
N(1)−Fe(1)−N(6)	100.1(4)	96.9(2)	98.7(3)	99.3(5)
N(2)−Fe(1)−N(3)	154.7(4)	166.3(2)	164.8(3)	160.7(5)
N(2)−Fe(1)−N(4)	76.8(4)	81.5(2)	80.9(3)	80.5(5)
N(2)−Fe(1)−N(5)	105.0(4)	95.6(2)	101.7(3)	103.5(5)
N(2)−Fe(1)−N(6)	79.8(4)	84.2(2)	82.6(3)	81.2(5)
N(3)−Fe(1)−N(4)	126.5(4)	111.5(2)	112.4(3)	116.6(5)
N(3)−Fe(1)−N(5)	85.7(4)	88.5(2)	85.6(3)	85.6(5)
N(3)−Fe(1)−N(6)	89.4(4)	91.9(2)	90.5(3)	89.9(5)
N(4)−Fe(1)−N(5)	91.9(4)	92.0(2)	91.8(3)	92.0(5)
N(4)−Fe(1)−N(6)	90.6(4)	87.1(7)	87.4(3)	88.8(5)
N(5)−Fe(1)−N(6)	175.0(3)	179.0(7)	175.5(3)	175.3(5)

[a] The hydrated salts crystallize in the *C*2/*c* space group where the cation occupies two different sites in the lattice, one on a general position and the other on a special position. Nitrogen atoms N(1) and N(2) in one cation and N(7) in the other are part of the ethylene linkage. [b] From the 173 K X-ray structure of [Fe(mtpen)](ClO$_4$)$_2$·$^2/_3$H$_2$O. [c] From the 298 K X-ray structure of [Fe(tpen)](ClO$_4$)$_2$. [d] From the X-ray structures (298 and 358 K) of [Fe(tpen)](ClO$_4$)$_2$·$^2/_3$H$_2$O.

Selected bond distances and angles for [Fe(mtpen)](ClO$_4$)$_2$·$^2/_3$H$_2$O are given in Table 3. The metal−ligand bond lengths are significantly longer than the low-spin nonsolvated [Fe(tpen)]-

$(ClO_4)_2$ complex or either of the two structures (298 or 358 K) of the solvated form. The average Fe−N_{aliph} distance of 2.17(1) Å and Fe−N_{py} distance of 2.15(2) Å for the $[Fe(mtpen)]^{2+}$ cation at the general position is consistent with high-spin Fe^{II}, as was anticipated from the magnetic data reported by Toftlund.[21] Interestingly, we do not see as marked a difference in geometric details between the general position and special position cations that we observed[20] for $[Fe(tpen)](ClO_4)_2 \cdot {}^2/_3H_2O$. When compared to the low-spin form of $[Fe(tpen)](ClO_4)_2$ (298 K), the FeN_6 octahedron of $[Fe(mtpen)](ClO_4)_2$ is more distorted in terms of bond angles in the first coordination sphere, see Table 3. An analysis of the structure of $[Fe(mtpen)](ClO_4)_2$ shows that the high-spin character of this molecule is likely due to steric interactions between the methyl group at the 6-position of the pyridyl ring and the *cis* pyridine rings bound to the Fe^{II} center. Molecular modeling studies show that rotation of the 6-methyl group about its local C_3 axis in the $[Fe(mtpen)](ClO_4)_2$ structure does not result in any significant van der Waals contact with neighboring atoms. However, when we took the $[Fe(tpen)](ClO_4)_2$ structure (low-spin form) and replaced the proton at the 6-position of *any* pyridyl group with CH_3, rotation of the methyl group results in H···C and H···N contacts of less than 1 Å. Thus, despite the fact that the donor strength of the pyridyl ring would be expected to increase upon methyl substitution at the 6-position and stabilize the $^1A_1$ state of the Fe^{II} complex, the steric crowding introduced by the methyl group prevents the pyridyl ring from approaching to a Fe−N_{py} distance of ∼2.0 Å required for a low-spin Fe−N bond. The result is a longer metal−ligand bond length and a $^5T_2$ ground state for $[Fe(mtpen)](ClO_4)_2$.

Probably the most important aspect of the structure of the $[Fe(mtpen)]^{2+}$ cation centers around the trigonal twist angles of this Fe^{II} complex. A comparison with $[Fe(tpen)]^{2+}$ is enlightening. In both complexes the fusion of the five-membered chelate rings, as well as the ethylenediamine linkage, result in marked deviations from octahedral symmetry. If we define the two trigonal planes according to the geometry of the ligand itself, that is, take one plane as N(1)−N(3)−N(4) and the other as N(2)−N(5)−N(6), two different types of trigonal twist angles can be defined as follows:

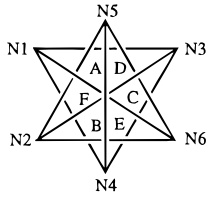

From the X-ray structure of the nonsolvated low-spin $[Fe(tpen)](ClO_4)_2$ the average trigonal twist of type I (A, B, and C) is found to be 49.5°, and for the type II trigonal twist (D, E, and F), the average angle is 70.5°. These are to be compared with the expected twist of 60° for a strictly octahedral complex. This substantial trigonal distortion ($\phi = 10.5°$) is reflected in the strained N(4)−Fe−N(1) and N(2)−Fe−N(6) angles of 81.0(2)° and 81.5(2)°, respectively, which cause the N(4)−Fe−N(6) angle to expand to 111.5(2)°. However, all four Fe−N_{py} distances are virtually identical to within 0.002 Å at 1.988 Å (av), and the two Fe−N_{aliph} distances are statistically identical [2.002(4) Å for FeN(1); 1.996(4) Å for Fe−N(2)]. The slightly shorter Fe−N_{py} distances are possibly due to some degree of π-back-bonding between the Fe center and the pyridine rings. All of these bond distances are similar to those observed for several other low-spin ferrous complexes and consistent with the results from magnetic studies indicating the low-spin configuration of $[Fe(tpen)](ClO_4)_2$ at room temperature.

Table 4. Trigonal Twist Angles[a]

compd	type I angle (deg)	type II angle (deg)
$[Fe(tpen)](ClO_4)_2$	49.5	70.5
$[Fe(tpen)](ClO_4)_2 \cdot {}^2/_3H_2O$ at 298 K	45.7	74.3
	49.5	70.4
$[Fe(tpen)](ClO_4)_2 \cdot {}^2/_3H_2O$ at 358 K	42.6	77.4
	46.7	73.3
$[Fe(mtpen)](ClO_4)_2 \cdot {}^2/_3H_2O$ at 173 K	37(2)	83(5)

[a] See the text for the definition of type I and type II trigonal twist angles. The hydrated salts each have two different cations in the unit cell.

In the structure of $[Fe(tpen)](ClO_4)_2 \cdot {}^2/_3H_2O$ there are two different cation sites (hereafter defined as site A and site B). Site A occurs as a general position, whereas cations at site B sit at special positions in the *C*2/*c* unit cell. The trigonal twist angles are quite different for the two sites at 298 K. The average type I angle (*vide supra*) for site A is 45.7°, while for site B cations this average is 49.5°. Similar differences are noted in the values for the type II angles: 74.3° for site A and 70.4° for site B. It is clear that the degree of trigonal distortion is larger for the site A molecules than for the site B molecules. The Fe−ligand atom distances are also larger for the site A cations. Thus, it appears that the small amounts of high-spin complexes present in $[Fe(tpen)](ClO_4)_2 \cdot {}^2/_3H_2O$ at 298 K are located at site A and these cations also have the greater trigonal twist.

In the 358 K X-ray structure of $[Fe(tpen)](ClO_4)_2 \cdot {}^2/_3H_2O$ there are also two different cation sites. With the increase in temperature from 298 to 358 K the fraction of high-spin complexes has grown to ∼40%. An examination of Table 3 shows that the Fe−ligand atom distances at 358 K are larger than those at 298 K. At 358 K the site A cations exhibit larger Fe−N bond lengths than the site B cations. As far as this paper is concerned, the important point to note is that compared to the 298 K structure, the trigonal twist angles for $[Fe(tpen)]^{2+}$ at 358 K indicate that the higher temperature structure is even more distorted along that coordinate: the type I angles are 42.6 and 46.7° for the A and B sites, respectively; the type II angles are found to be 77.4 and 73.3° (*i.e.*, $\phi = 17.4°$ for A and $\phi = 13.3°$ for B).

In Table 4 the trigonal twist angles for the various tpen structures are collected. From the data on the $[Fe(tpen)]^{2+}$ structures it is seen that the degree of torsional distortion away from idealized octahedral symmetry increases with increasing high-spin content in the tpen complex. This trend continues with the totally high-spin $[Fe(mtpen)](ClO_4)_2 \cdot {}^2/_3H_2O$. Type I angles for the cation average 37(2)°, while type II angles are 83(5)°, representing a significant decrease in the value of ϕ relative to the 358 K structure of $[Fe(tpen)](ClO_4)_2 \cdot {}^2/_3H_2O$. This result firmly establishes that, in addition to the expected increase in metal−ligand bond lengths accompanying the low-spin to high-spin conversion [$\Delta r_{av} = 0.17(1)$ Å in this system], there is a substantial change in the extent of distortion along torsional coordinates, in particular about the pseudo-C_3 axis of the octahedron. Since the data on changing metal−ligand bond lengths were the principal reason why the symmetric breathing mode was believed to be coupled to the kinetics of spin-state interconversion, our structural study on $[Fe(tpen)]^{2+}$ and $[Fe(mtpen)]^{2+}$ suggests that lower frequency torsional modes should be given very serious consideration as a possible reaction coordinate for the spin-crossover transformation.

X-ray Crystal Structure of $[Fe(tppn)](ClO_4)_2 \cdot H_2O$. The ligand tppn is very closely related to tpen; it can be considered as a minor perturbation on the tpen structure involving methylation of the ethylenediamine backbone. The chelation to the

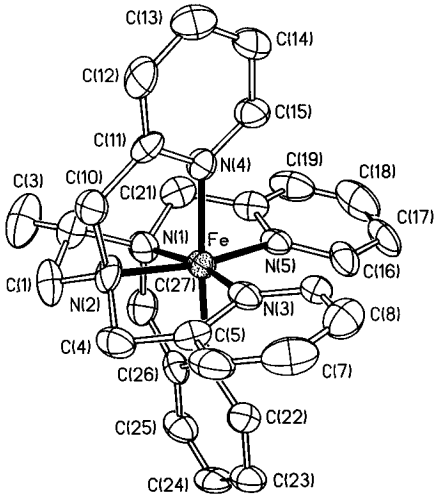

Figure 3. ORTEP drawing of the $[Fe(tppn)]^{2+}$ cation in the structure of $[Fe(tppn)](ClO_4)_2 \cdot H_2O$.

Table 5. Selected Bond Distances and Angles for $[Fe(tppn)](ClO_4)_2 \cdot H_2O$

	Distances (Å)		
Fe−N(1)	1.988(13)	Fe−N(2)	1.993(9)
Fe−N(3)	1.976(11)	Fe−N(4)	1.987(9)
Fe−N(5)	2.003(9)	Fe−N(6)	2.000(9)
	Angles (deg)		
N(1)−Fe−N(2)	87.6(4)	N(1)−Fe−N(3)	167.4(4)
N(2)−Fe−N(3)	81.1(4)	N(1)−Fe−N(4)	97.8(4)
N(2)−Fe−N(4)	83.6(4)	N(3)−Fe−N(4)	86.4(4)
N(1)−Fe−N(5)	81.5(4)	N(2)−Fe−N(5)	167.6(5)
N(3)−Fe−N(5)	110.4(4)	N(4)−Fe−N(5)	92.2(4)
N(1)−Fe−N(6)	82.2(4)	N(2)−Fe−N(6)	99.0(4)
N(3)−Fe−N(6)	92.1(4)	N(4)−Fe−N(6)	176.9(4)

metal center about the pseudo-C_2 axis is still a five-membered ring, so it is not too surprising that many of the macroscopic properties of $[Fe(tppn)](ClO_4)_2$ bear close resemblance to $[Fe(tpen)](ClO_4)_2$. The magnetic properties of $[Fe(tppn)](ClO_4)_2$ in the solid state have been previously reported by Toftlund.[21] The data reveal that the $T_{1/2}$ of $[Fe(tppn)](ClO_4)_2$ is slightly higher than for $[Fe(tpen)](ClO_4)_2 \cdot {}^2/_3H_2O$ ($T_{1/2} \simeq 385$ K), but still the tppn complex exhibits the spin-crossover in an accessible temperature range. The single-crystal X-ray structure was determined for this compound. The compound crystallizes in the monoclinic space group $P2_1/n$ with $Z = 4$, which is very similar to the nonsolvated form of $[Fe(tpen)](ClO_4)_2$.[20] Selected bond distances and angles are given in Table 5. An ORTEP drawing of the cation is shown in Figure 3. Essentially there is little difference between the metric details of $[Fe(tppn)](ClO_4)_2 \cdot H_2O$ and the predominantly low-spin form of $[Fe(tpen)](ClO_4)_2$. The average Fe−N bond distances are 1.990(5) Å for the aliphatic nitrogen atoms and 1.99(1) Å for the pyridyl nitrogen atoms; both are consistent with low-spin Fe^{II}. The angles about the octahedron are also relatively unremarkable, showing distortions from octahedral symmetry similar to $[Fe(tpen)](ClO_4)_2$. One curious feature of the structure is a static disorder in the location of the terminal methyl group of the 2-pyridylamine fragment [found either at C(1) or C(2)]. The similarity between $[Fe(tpen)]^{2+}$ and $[Fe(tppn)]^{2+}$ will carry through the kinetic studies, as well (*vide infra).*

Physical Properties of $[Fe(tptn)](ClO_4)_2$ in the Solid State. In contrast to tppn, it was anticipated that the tptn complex with Fe^{II} will display physical properties distinct from $[Fe(tpen)](ClO_4)_2$. This expectation is borne out by data reported by Toftlund in 1981.[21] The magnetic susceptibility of $[Fe(tptn)](ClO_4)_2$ is temperature-independent up to ~400 K with $\mu_{eff} \approx 0.5\mu_B$, indicating that this complex is fully low-spin over the entire temperature range studied. Since the inductive effects on the donor strength of the aliphatic nitrogen atoms will be approximately the same for tppn and tptn, the fact that tptn is completely low spin cannot be readily explained in these terms. It is likely that the strain introduced by the five-membered chelate rings of both tpen and tppn lowers the effective ligand field strength of those ligands relative to tptn. The six-membered chelate ring formed when tptn binds will be less strained, resulting in better σ-based donation.

The change in chelation anticipated with the introduction of a six-membered ring in the coordination sphere of Fe^{II} makes the structure of $[Fe(tptn)](ClO_4)_2$ of great interest, particularly with respect to torsional angles about the pseudo-C_2 axis. Large single crystals were obtained of this compound by slow evaporation of a MeOH solution of $[Fe(tptn)](ClO_4)_2$. Unfortunately, we have been unable to determine the structure of this compound despite collecting an entire hemisphere of what appears to be high-quality data. It is known that the complex crystallizes in a hexagonal space group, and the observed systematic absence of 00l (l = 6*n*) indicates that the space group is one of $P6_5$, $P6_1$, $P6_522$, or $P6_122$. We were able to determine the unit cell parameters from these data. The experimentally measured density of 1.51(3) g cm^{-3} coupled with the unit cell volume of *ca*. 7000 Å^3 indicates $Z = 9$ based on the molecular weight of $[Fe(tptn)](ClO_4)_2$. This value for Z is consistent with either $P6_522$ or $P6_122$ by placing one molecule at a general position and one molecule on a 2-fold rotation axis and does tend to discount $P6_5$ and $P6_1$ as possibilities. Given only this information, there is very little else that can be said concerning the structure of this compound. We will rely on the indication from the magnetic data that the six-membered ring relaxes the overall structure of the cation and that this presumably translates into a torsional angle ϕ that is closer to the octahedral value of 60° than either $[Fe(tpen)]^{2+}$ or $[Fe(tppn)]^{2+}$.

Variable-Temperature Kinetics in the tpen Series. Variable-temperature kinetic data have been collected on several molecules, including $[Fe(tppn)](ClO_4)_2$, $[Fe(tpen)](ClO_4)_2$, $[Fe(tptn)](ClO_4)_2$, and $[Fe(dpa)_2](ClO_4)_2$. Data collected on $[Fe(t\text{-tpchxn})](ClO_4)_2$ are reported in a separate paper.[19] The temperature-dependence of the ${}^5T_2 \rightarrow {}^1A_1$ relaxation rate was measured for all of the above complexes. The goal of this research was to examine whether the activation energy for the ${}^5T_2 \rightarrow {}^1A_1$ relaxation correlates with the "ease" of trigonal twisting motion in each complex.

Variations in the tpen series primarily occur in the backbone structure that connects the two "halves" of the ligands in this system, where the pseudo-C_2 axis represents a bisection of the backbone and distortion occurs along the Θ coordinate. For example, in both $[Fe(tpen)](ClO_4)_2$ and $[Fe(tppn)](ClO_4)_2$ the backbone involves a five-membered chelate ring when bound to the metal center, whereas for the isomer $[Fe(tptn)](ClO_4)_2$ the chelate is a six-membered ring which should in general be more flexible. $[Fe(dpa)_2](ClO_4)_2$ represents an extreme in geometric flexibility, where the hexadentate ligand has in effect been cut in two, allowing for free rotation of the two trigonal faces with respect to one another. With this kind of information in mind, we shall attempt to see if any correlation exists between what is known structurally about these systems with the parameters that characterize the kinetics of spin-state interconversion.

The kinetics for $[Fe(tpen)](ClO_4)_2$ were determined following excitation at $\lambda_{pump} = 440$ nm while monitoring at $\lambda_{probe} = 414$ nm, which is the maximum of the ${}^1MLCT \leftarrow {}^1A_1$ absorption band. As with all of the molecules to be discussed, *the kinetics*

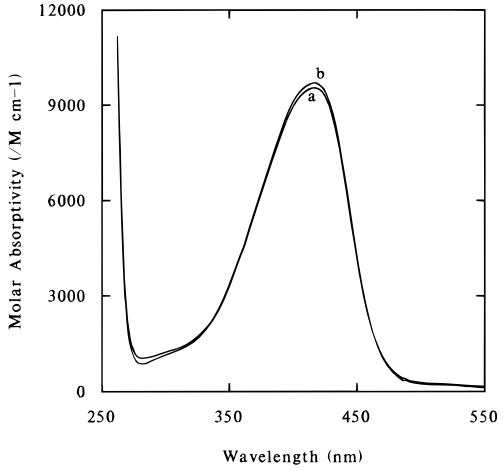

Figure 4. Plot of the electronic absorption spectrum of [Fe(tpen)]-$(ClO_4)_2$ in MeOH before (a) and after (b) variable-temperature laser photolysis.

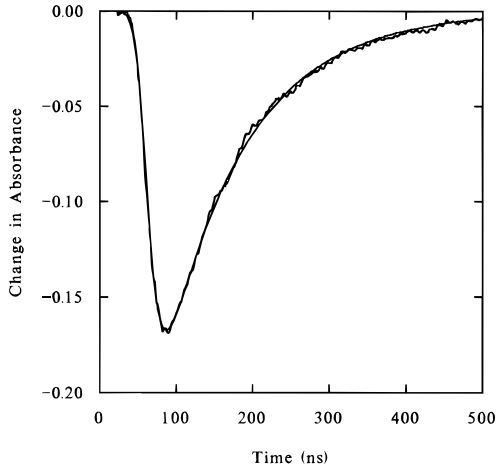

Figure 5. Profile of transient decay for [Fe(tpen)]$(ClO_4)_2$ in MeOH (2.52×10^{-4} M) monitored at 414 nm following excitation at 440 nm. Data were collected at 220 K. The smooth solid line represents a convolution of the instrument response function with a single-exponential decay, where $\tau_{obs} = 109$ ns.

were found to be independent of both pump and probe wavelengths over the entire range spanned by the ^{1}*MLCT* ← $^1A_1$ absorption band. All of the data for molecules in the tpen series were collected on MeOH solutions of the complexes at concentrations of $(2.5 \pm 0.1) \times 10^{-4}$ M. Figure 4 shows that photolysis resulted in no significant degradation of a MeOH solution of the tpen complex, as evidenced by the absorption spectrum of the solution before and after the variable-temperature experiment. Photodegradation was not a problem for any of the molecules studied. A typical single-wavelength kinetic trace of the relaxation of [Fe(tpen)]$(ClO_4)_2$ in a 2.52×10^{-4} M (3.21×10^{-4} m) MeOH solution following photoexcitation is shown in Figure 5; these data were collected at $T = 220$ K. The solid line represents a convolution of the instrument response function with a single-exponential decay of the form given in eq 1, where A is premultiplier term, t is time, and τ_{obs}

$$\text{change in absorbance} = \Delta(\text{OD}) = A \exp\left\{-\frac{t}{\tau_{obs}}\right\} \quad (1)$$

is the observed lifetime. At $T = 220$ K, the value for the observed τ_{obs} was found to be 109 ns. Since integral deconvolution takes into account the entire pulse profile, we see from Figure 5 that both the rise and decay of the signal are fit in determining the value of the observed lifetime. Our interest in these studies is in the $^5T_2 \rightarrow {}^1A_1$ rate constant, k_{-1}. Since the value of K_{eq} is vanishingly small at this temperature, it can be shown[19] that eq 2 holds:

$$k_{-1} = \frac{k_{obs}}{(K_{eq}+1)} = \frac{1}{\tau_{obs}(K_{eq}+1)} \simeq \frac{1}{\tau_{obs}} = 9.17 \times 10^6\ \text{s}^{-1} \quad (2)$$

In this first paper each variable-temperature data set is fit to both the Arrhenius and Eyring models.

The activation energy, E_a, for the $^5T_2 \rightarrow {}^1A_1$ relaxation process for [Fe(tpen)]$(ClO_4)_2$ in methanol is 767 ± 22 cm^{-1} with an intercept (*i.e.*, frequency factor) of $(1.35 \pm 0.2) \times 10^9$ s^{-1}. The corresponding parameters from the fit of an Eyring plot (eq 3)

$$k_{-1} = \frac{\kappa k_B T}{h} \exp\left\{\frac{-\Delta S^{\ddagger}}{R}\right\} \exp\left\{\frac{-\Delta H^{\ddagger}}{RT}\right\} \quad (3)$$

(modified by the introduction of a transmission coefficient κ as a premultiplier) are $\Delta H^{\ddagger} = 604 \pm 25$ cm^{-1} with an intercept of 14.6 ± 0.2. $\Delta H^{\ddagger}$ is the enthalpy of activation for the transition state. The y-intercept from a plot of ln (k/T) versus T^{-1} is nominally a sum of several terms as given in the temperature-independent portion of the equation. We have chosen to express the intercept from all Eyring plots as a sum of two terms, namely [ln (κ) + $\Delta S^{\ddagger}$/R], giving a value of -9.2 ± 0.1 in the case of [Fe(tpen)]$(ClO_4)_2$ in MeOH. Generally data on spin-state interconversion rates[25] have been analyzed in terms of transition state theory by assuming a value for the transmission coefficient κ in order to obtain a "value" for the entropy of activation for the transition state $\Delta S^{\ddagger}$. An assignment of $\kappa = 1$ implies that the $^5T_2 \rightarrow {}^1A_1$ process is adiabatic. This is unlikely and more realistic estimates place its value at $\sim 10^{-2}$. The value of $\Delta S^{\ddagger}$ will reflect changes in both the electronic and vibrational partition functions that must accompany the spin change. In addition, this term will also contain contributions from changes in the solvation entropy, a number which could be either positive or negative. Rather than impose an assumed value on either of these parameters, we simply report the sum of the two terms and do not elaborate further on the relative contributions from either κ or $\Delta S^{\ddagger}$.

It should be pointed out that the error bars quoted on activation parameters throughout this paper represent 2σ for the least-squares linear regression analysis *only*. No attempt has been made to incorporate the error associated with the measured lifetimes, the temperature, or the ln K_{eq} versus T^{-1} linear regression used to evaluate K_{eq} for the temperatures used in the laser experiment. Since the value of K_{eq} is so small in these systems and only comes into play for the highest temperature data points, the error introduced by this latter term is negligible. With our two-diode configuration we feel that the temperature values have an estimated precision of better than ± 1 K, while the absolute accuracy is probably ± 2 K. The rate constants are the most critical error source in the experiment. The time base of the digitizer was calibrated with a 1.000 MHz crystal to better than $\pm 0.4\%$ prior to each experiment. However, the relative precision for each data point is somewhat a function of the value of the observed lifetime itself. For lifetimes longer than the *ca*. 40 ns instrument response function, error bars of $\pm 5-7\%$ appear to be quite reasonable. For $\tau_{obs} < 40$ ns, a fixed error of ± 2 ns is appropriate. We think that a fair representation of our variable-temperature fits to the Arrhenius and Eyring models would be to consider errors bars of $2\sigma +$ 100%. This is likely an overestimate of the error.

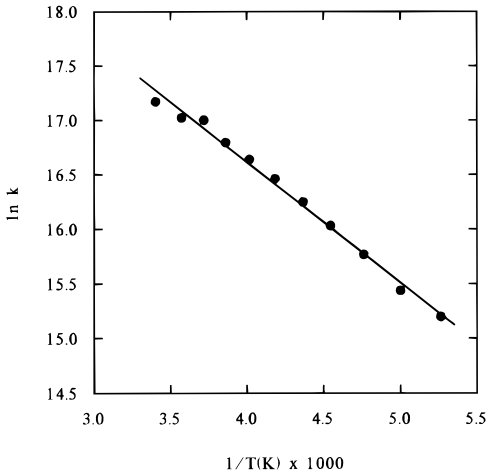

Figure 6. Arrhenius plot of relaxation data for $[Fe(tppn)](ClO_4)_2$ collected in MeOH at a concentration of 2.58×10^{-4} M. The solid line represents a best-fit linear least-squares regression of the data.

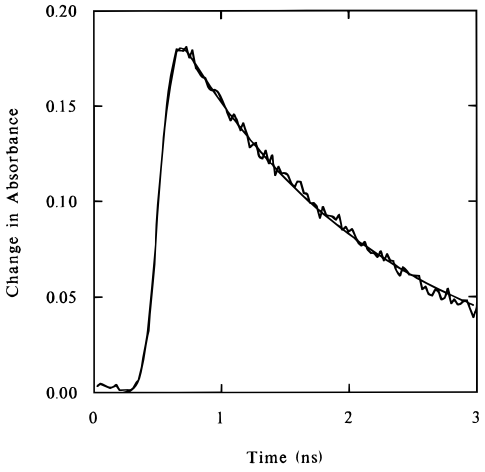

Figure 7. Profile of transient decay for $[Fe(tptn)](ClO_4)_2$ in H_2O (1.57×10^{-3} M) monitored at 266 nm following excitation at 355 nm. These data were collected at 295 K on a picosecond spectrometer having a pulse width of 80 ps. The smooth solid line represents a convolution of the instrument response function with a single-exponential decay, where $\tau_{obs} = 1.6$ ns.

Laser flash kinetic data were also collected on a 2.58×10^{-4} M (3.27×10^{-4} m) MeOH solution of $[Fe(tppn)](ClO_4)_2$. The Arrhenius plot of the k_{-1} data in Figure 6 was fit to give an activation energy of 771 ± 17 cm^{-1} with a frequency factor of $(1.45 \pm 0.2) \times 10^9$ s^{-1}. The corresponding thermodynamic parameters from a fit of the same data to eq 3 are $\Delta H^{\ddagger} = 608 \pm 20$ cm^{-1} and $(\ln \kappa + \Delta S^{\ddagger}/R) = -9.13 \pm 0.08$. The fitting parameters for this tppn complex are virtually identical to those obtained for $[Fe(tpen)](ClO_4)_2$ in MeOH. This is perhaps not too surprising given the subtle structural differences afforded by changing from a 1,2-propylenediamine backbone to a 1,2-ethylenediamine backbone. The *ca.* 770 cm^{-1} activation energy found for both $[Fe(tpen)](ClO_4)_2$ and $[Fe(tppn)](ClO_4)_2$ is quite small: upon increasing the temperature from 190 to 294 K in $[Fe(tpen)](ClO_4)_2$, for example, the value of k_{-1} increases by less than an order of magnitude (4.00×10^6 to 2.87×10^7 s^{-1}). In a semiclassical sense, the observation of a small activation energy given the large degree of nuclear reorganization that accompanies the spin change suggests that the majority of the nuclear displacement for the reaction occurs as vibrational relaxation after the system has already crossed onto the potential energy surface of the product and completed the reaction. This is an interesting interpretation in light of Purcell's suggestion[15] that only a fraction of the total displacement along a low-frequency torsional coordinate would be required to induce a spin change in a pseudo-octahedral system.

One critical similarity between $[Fe(tpen)](ClO_4)_2$ and $[Fe(tppn)](ClO_4)_2$ is that both complexes bind to Fe^{II} by forming a five-membered chelate ring that links the two trigonal faces of the octahedron. A reasonable approach, then, would be to examine the effect of changing the nature of this chelation on the kinetics. This is achieved with the compounds $[Fe(tptn)](ClO_4)_2$ and $[Fe(dpa)_2](ClO_4)_2$. The first complex is convenient for comparative purposes in that it is a structural isomer of $[Fe(tppn)](ClO_4)_2$ with regard to the bridging backbone (1,3-propylenediamine in tptn versus 1,2-propylenediamine in tppn). In $[Fe(tptn)](ClO_4)_2$, an all low-spin complex, chelation of the ligand produces a six-membered ring with respect to the trigonal backbone. The second compound, $[Fe(dpa)_2](ClO_4)_2$, is also low-spin at all temperatures studied and represents the case where rotation of the two trigonal faces is relatively unhindered.

Laser flash kinetic data were collected on a 2.54×10^{-4} M (3.21×10^{-4} m) MeOH solution of $[Fe(tptn)](ClO_4)_2$. The observed lifetime at $T = 191$ K of $\tau_{obs} \approx 14$ ns is more than an order of magntiude shorter than that measured for $[Fe(tppn)](ClO_4)_2$ at the same temperature ($\tau_{obs} = 244$ ns). We were only able to collect data on this compound up to $T = 210$ K owing to the very small signal produced by the short-lived species. Since these data are admittedly of low quality due to the magnitude of the rate constant, we measured the relaxation of this system at room temperature using a picosecond spectrometer. Excitation at $\lambda_{pump} = 355$ nm produced the transient decay curve shown in Figure 7 at $\lambda_{probe} = 266$ nm. At this wavelength the excited state has a stronger absorbance than the ground state, so a transient absorption is observed rather than a transient bleach. However, identical results were found for a transient bleach observed in this system at $\lambda_{probe} = 440$ nm; τ_{obs} at all probe wavelengths was measured to be 1.6 ± 0.1 ns. It should be noted that the data shown in Figure 7 were obtained on a 1.57×10^{-3} M aqueous solution of $[Fe(tptn)](ClO_4)_2$ as opposed to the 2.54×10^{-4} M MeOH solution used for the low-temperature studies. However, we have determined that the $^5T_2 \rightarrow {}^1A_1$ dynamics of these systems are both solvent and concentration independent. The linear regression analysis of the data on $[Fe(tptn)](ClO_4)_2$, including the picosecond data at room temperature, gives $E_a = 777 \pm 50$ cm^{-1} with a frequency factor of $(2.6 \pm 0.8) \times 10^{10}$ s^{-1} [$\Delta H^{\ddagger} = 613 \pm 47$ cm^{-1}, and $(\ln \kappa + \Delta S^{\ddagger}/R) = -6.3 \pm 0.1$]. Thus, the activation energies of the tpen, tppn, and tptn complexes are identical within experimental error.

Data were also collected on a 2.52×10^{-4} M (3.20×10^{-4} m) MeOH solution of $[Fe(dpa)_2](ClO_4]_2$. In Figure 8 is shown the Arrhenius plot of the data. The activation energy of 339 ± 13 cm^{-1} ($\Delta H^{\ddagger} = 179 \pm 13$ cm^{-1}) is extremely small; the rate constant for the $^5T_2 \rightarrow {}^1A_1$ conversion increases by less than a factor of 2.5 over the temperature range studied (1.93×10^7 s^{-1} at 191 K to 4.59×10^7 s^{-1} at 282 K). The value of E_a is more than a factor of 2 smaller than was observed for the hexadentate-ligated complexes discussed above. This is a strong indication that the ligand structure is very influential in determining the value of the activation energy. The fact that the activation energy *decreases* upon cleavage of the chelate backbone suggests that allowing unrestricted motion of the two trigonal faces of the polyhedron makes it much easier for the system to convert from the high-spin state to the low-spin state. In contrast, spin interconversion in $[Fe(t\text{-}tpchxn)]^{2+}$, a molecule representing the other extreme in structural flexibility with its fused-ring backbone, exhibits a ca. 2300 cm^{-1} barrier for $^5T_2 \rightarrow {}^1A_1$ relaxation.[19] These results are precisely what we would expect if the dynamics of a torsional mode (*e.g.*, twisting of

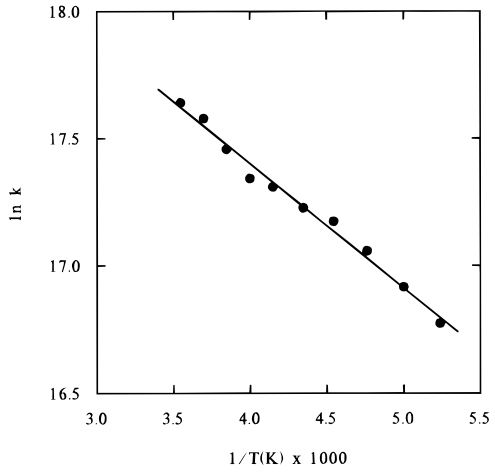

Figure 8. Arrhenius plot of relaxation data for $[Fe(dpa)_2](ClO_4)_2$ collected in MeOH at a concentration of 2.52×10^{-4} M. The solid line represents a best-fit linear least-squares regression of the data.

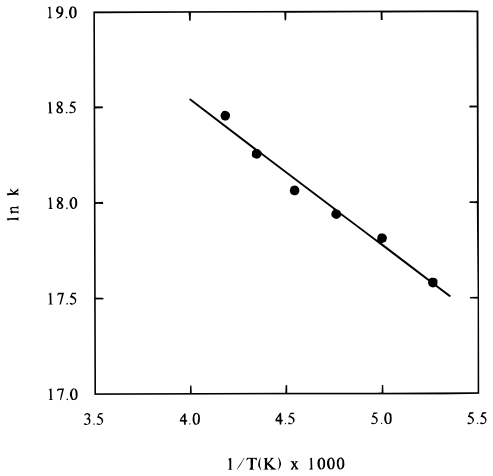

Figure 9. Arrhenius plot of relaxation data for $[Fe(terpy)_2](ClO_4)_2$ collected in MeOH at a concentration of 4.0×10^{-4} M. The solid line represents a best-fit linear least-squares regression of the data.

the trigonal faces with respect to each other) were controlling the kinetics of the spin-crossover transformation.

In addition, we note a *substantial* change in the frequency factor between $[Fe(dpa)_2](ClO_4)_2$ and $[Fe(tptn)](ClO_4)_2$. The frequency factor for the $^5T_2 \rightarrow {}^1A_1$ conversion in $[Fe(dpa)_2](ClO_4)_2$ of $(2.5 \pm 0.25) \times 10^8$ s^{-1} is approximately 2 orders of magnitude smaller than the frequency factor of $[Fe(tptn)](ClO_4)_2$. Whereas the increase in frequency factor between $[Fe(tptn)](ClO_4)_2$ and the tpen/tppn complexes could be attributed to the larger $^1A_1/^5T_2$ gap in $[Fe(tptn)](ClO_4)_2$, the same rationalization *cannot* be used to account for the frequency factor obtained for $[Fe(dpa)_2](ClO_4)_2$ since it too is a low-spin complex. The frequency factor can be viewed as the "intrinsic" rate of the reaction being modeled; it represents the rate in the limit as E_a approaches zero. Since this rate for $[Fe(dpa)_2](ClO_4)_2$ is slower than that for the tpen, tppn, and tptn complexes, molecules with equal or *smaller* $^1A_1/^5T_2$ energy gaps, we must conclude that another factor is strongly influencing the intrinsic rate of $^5T_2 \rightarrow {}^1A_1$ conversion.

At first glance the slower intrinsic rate for $[Fe(dpa)_2](ClO_4)_2$ would appear to be inconsistent with the twisting model, since the possibility of unhindered rotation about the pseudo-C_3 axis of the octahedron would presumably translate into a large intrinsic rate for conversion along that coordinate. This is not what is observed. To understand this result in the context of the torsional model, we refer back to the suggestion by Purcell[15] that only a slight displacement along the torsional coordinate would be *required* to effect the spin transformation. In his analysis of the interaction between the high-spin and low-spin states Purcell indicated that the greater the extent of trigonal distortion, the larger the degree of mixing of the $^1A_1$ and $^5T_2$ states with the $^3T_1$ state. In this sense, it is perhaps best to think of the magnitude of the interaction between the $^1A_1$ and $^5T_2$ states as being dynamic. That is, if the distortion coupled to the spin-conversion process is modulating the extent of mixing, the interaction between the two states will be constantly changing during the course of the reaction. The 2 $|H_{ab}|$ separation between the upper and lower surfaces of the nonadiabatic potential would then be a function of ΔQ, the extent of distortion. The value we attribute to H_{ab} might be appropriate at the transition state, but this value would represent the maximum for the overall process; in reality H_{ab} would be increasing as the system approached the nuclear configuration corresponding to the transition state and then would decrease as the system relaxed in the product well.

According to this dynamical model for the value of H_{ab}, small displacements result in small intrinsic rate constants relative to a larger displacement along the same coordinate. We suggest that the small intrinsic rate for $[Fe(dpa)_2](ClO_4)_2$ is actually due to the unhindered motion along the torsional coordinate that takes full advantage of fact that all that is minimally needed to achieve the conversion from the high-spin state to the low-spin state is a small displacement. The value of H_{ab} at the transition state configuration, which effectively determines the rate in the limit of E_a approaching zero, correlates with the displacement along the reaction coordinate and is therefore small for this system.

Kinetic Studies on Other Systems. Results that have been obtained on several "classic" iron(II) polypyridyl complexes will be briefly mentioned. These molecules do not fit in well with the geometric concept behind the tpen series, but they are nonetheless interesting in their own right. We have chosen to re-examine three complexes that were previously studied at room temperature by Creutz *et al*. in their classic 1980 paper.[26] Variable-temperature relaxation data were collected on a 4.0×10^{-4} M (5.1×10^{-4} m) MeOH solution of $[Fe(terpy)_2](ClO_4)_2$, where terpy is 2,2′,6′,2″-terpyridine. The Arrhenius plot of the data is shown in Figure 9. Due to the magnitude of the rate constant we were unable to collect any data at temperatures above 240 K with our nanosecond spectrometer. The activation energy of 532 ± 36 cm^{-1} ($\Delta H^{\ddagger} = 384 \pm 34$ cm^{-1}) suggests a lifetime of ~5 ns at 295 K, slightly different from the value of 2.54 ns quoted by Creutz *et al*.[26] at room temperature in aqueous solution but still in reasonable agreement given the weak signals observed in our experiment.

Data were also collected at room temperature on aqueous solutions of $[Fe(bpy)_3](ClO_4)_2$ and $[Fe(phen)_3](ClO_4)_2$ using the picosecond laser spectrometer. The observed transient decay profile for $[Fe(bpy)_3](ClO_4)_2$ photoexcited at $\lambda_{pump} = 532$ nm and monitored at $\lambda_{probe} = 440$ nm is shown in Figure 10. The lifetime of the $^5T_2 \rightarrow {}^1A_1$ conversion was found to be 676 ± 30 ps ($k_{-1} = (1.48 \pm 0.07) \times 10^9$ s^{-1}) in the case of $[Fe(bpy)_3](ClO_4)_2$ and 685 ± 30 ps ($k_{-1} = (1.46 \pm 0.07) \times 10^9$ s^{-1}) for $[Fe(phen)_3](ClO_4)_2$. The values are only slightly different from the 810 ± 70 and 800 ± 70 ps values reported by Creutz *et al*.[26] and agree with their conclusion that the lifetimes for the two complexes are identical within experimental error. One might have expected differences between these two compounds

(26) Creutz, C.; Chou, M.; Netzel, T. L.; Okumura, M.; Sutin, N. *J. Am. Chem. Soc.* **1980**, *102*, 1309.

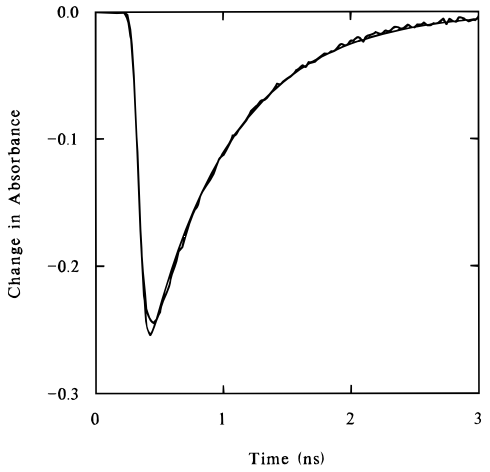

Figure 10. Profile of transient decay for $[Fe(bpy)_3](ClO_4)_2$ in H_2O (8.2×10^{-4} *M*) monitored at 440 nm following excitation at 532 nm. These data were collected at room temperature using a picosecond spectrometer having a pulse width of 80 ps. The smooth solid line represents a convolution of the instrument response function with a single-exponential decay, where $\tau_{obs} = 676$ ps.

on the basis of an energy gap dependence since the ligand field strengths of bpy and phen are not identical. However, this dependence is not observed experimentally. We attempted to collect relaxation data on $[Fe(bpy)_3](ClO_4)_2$ in MeOH solution at 190 K but were unable to see any appreciable signal at this temperature. This places an upper limit of the lifetime of the $^5T_2$ state in $[Fe(bpy)_3](ClO_4)_2$ at *ca.* 1 ns at 190 K, consistent with the near-barrierless excited-state relaxation predicted by Sutin.[27]

Concluding Comments

The preparations, X-ray structures, and the results of laser-flash photolysis studies of a series of Fe^{II} complexes are reported. In the series there are variations in the hexadentate ligand engineered to provide changes in the trigonal twist of the octahedral complex. It was of interest to see if the trigonal twisting characteristics impacted on the rate of $^5T_2 \rightarrow {}^1A_1$ intersystem crossing for the Fe^{II} complexes. X-ray structural results were presented for two of the Fe^{II} complexes, and together with X-ray results we presented previously for other complexes in the series, it is clearly established that for a given complex or for a series of similar complexes not only do the metal−ligand bond distances increase with increasing high-spin content, but the degree of trigonal twisting also increases with increasing high-spin content. Thus, when the temperature of a crystal of a spin crossover complex is increased such that it goes from low spin to high spin, it is found that the trigonal twist angle increases.

The laser-flash photolysis technique was used to measure the $^5T_2 \rightarrow {}^1A_1$ relaxation rates for several of the Fe^{II} complexes in MeOH in the range of 190−300 K. Linear Arrhenius plots were obtained which could be fit for the activation energy E_a and the frequency factor. It was found that an empirical correlation exists between the Arrhenius activation energy for $^5T_2 \rightarrow {}^1A_1$ relaxation and the flexibility of the ligand framework along a torsional coordinate. Specifically, we observed that the greater the extent of rotational freedom about the pseudo-C_2 axis of the octahedron, the smaller the activation energy for $^5T_2 \rightarrow {}^1A_1$ relaxation.

Conclusions were also drawn with regard to the frequency factor, which we interpret as the "intrinsic rate" of relaxation, *i.e.*, the rate in the limit of zero activation energy. The trend observed is counterintuitive at first glance, since it opposes the trend in E_a. However, the variations in the intrinsic rate could be understood in the context of a model which describes coupling of the $^1A_1$ and $^5T_2$ states as a dynamic quantity. Due to the fact that the $^1A_1$ and $^5T_2$ states couple via a second-order interaction with $S = 1$ state(s) whose energies are a *function of the reaction coordinate*, the parameter H_{ab} and hence the intrinsic rate of $^5T_2 \rightarrow {}^1A_1$ relaxations are functions of ΔQ. Thus, a molecule such as $[Fe(dpa)_2](ClO_4)_2$ which has no steric hindrance to torsional motion can undergo the minimum amount of distortion necessary to undergo surface crossing. More rigid systems such as $[Fe(tptn)](ClO_4)_2$ and $[Fe(t\text{-}tpchxn)](ClO_4)_2$ will distort to a different extent due to the conformational requirement of the ligand framework.

The data presented above certainly suggest that torsional mode(s) play a central role in controlling the kinetics of spin-state interconversion. However, these empirical correlations are not compelling enough to unequivocally establish the importance of these low-frequency modes in the molecular mechanism of spin crossover. In a later paper we will present a theoretical analysis of the kinetic data in terms of classical and quantum-mechanical theories of electron transfer. The conclusions drawn there, in conjunction with the empirical correlations outlined above, serve to strengthen our proposal that we need to abandon the single configurational coordinate model for spin-state interconversion wherein the symmetric stretching mode is the dominant reaction coordinate.

Acknowledgment. This work was supported by NSF Grant CHE-9420322 (D.N.H.) and NIH Grant HL-13652 (D.N.H.). The authors would like to thank Dr. Robert Dunn and Professor John Simon for help with the picosecond experiments.

Supporting Information Available: Complete listings of bond lengths and angles, anisotropic thermal parameters and hydrogen atom coordinates for $[Fe(mtpen)](ClO_4)_2 \cdot {}^2/_3H_2O$ at 173 and 296 K and $[Fe(tpen)](ClO_4)_2 \cdot {}^2/_3H_2O$ at 296 K (33 pages). See any current masthead page for ordering information instructions.

IC9507880

(27) Sutin, N. *Acc. Chem. Res.* **1982**, *15*, 275.